Ecological Indicators 127 (2021) 107712

Contents lists available at ScienceDirect

Ecological Indicators

journal homepage: www.elsevier.com/locate/ecolind

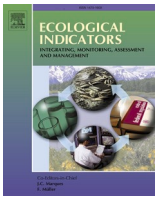

# Spatiotemporal characteristic and forecast of drought in northern Xinjiang, China

Haiwei Zhang [a,b], Jia Song [c,d,*], Gang Wang [a,b,e], XiuYi Wu [a,b], Jun Li [a,b]

[a] School of Geographical Sciences, Nanjing Normal University, Nanjing 210023, China
[b] Key Laboratory of Virtual Geographic Environment (Nanjing Normal University), Ministry of Education, Nanjing 210023, China
[c] State Key Laboratory of Hydrology-Water Resources and Hydraulic Engineering, Hohai University, Nanjing 210098, China
[d] College of Hydrology and Water Resources, Hohai University, Nanjing 210098, China
[e] School of Urban and Plan, Yancheng Teachers University, Yancheng 224002, China

ARTICLE INFO

*Keywords:*
Drought
Spatiotemporal Characteristic
Climate change
Wavelet Variance
SPEI

ABSTRACT

Understanding monitor accurately and predicting drought conditions are necessary to prevent economic losses and natural disasters. Now, there is still a lack of comprehensive assessment of drought prediction in Xinjiang. In order to better predict the future drought trend, firstly we analyzed the trends of SPEI and the magnitude and frequency of drought in selected surface meteorological stations from 1960 to 2017. Secondly, we compared drought trends and spatial distribution characteristics of SPEI and PDSI. Based on historical data from 1960 to 2017, the paper predicted the trends of SPEI and PDSI in the next five years. The results show that the winter SPEI has risen significantly, and there was a SPEI value mutation in 1994. The Spring, Summer and Autumn SPEI show an insignificant downward trend. It is relatively stable on other time scales , and there is no significant sudden change. It is inferred thatthe increasing trend of wetting that may occur under different time scales at NRX in 2021, winter and annual scales will continue to be humidified, and spring, summer, and autumn will continue to be arid. Droughts in NRX occur at least once every three years, which is a high frequency event. The prediction results of the artificial neutral network (ANN) method based on multilayer feed forward network show that probability of humidification at NRX is more likely in the future, and the prediction results of wavelet and Hurst index are basically consistent with that of ANN method.

## 1. Introduction

In recent years, as the global temperature continues to rise and the frequency of extreme weather events such as extreme precipitation and extremely high temperatures in local areas have been increasing (Dai, 2013; Dubrovsky et al., 2009). China is also a country seriously affected by drought disasters, especially in northern Xinjiang, North China, and Northeast China. Due to the influence of the continental climate and monsoon climate, the intensity and frequency of drought disasters in these regions are higher than that in other regions (Zhou et al., 2014; Shi et al., 2003; Wang et al., 2020).

Xinjiang is located in the interior of the mainland, with dry air, leading to severe restrictions on water resources, and climate change exacerbates the region's vulnerability in terms of water shortage (Li et al., 2017). Climate change in Xinjiang is both highly complex and highly sensitive to global warming (Chen et al., 2012; Chen and Sun, 2015). Affected by natural geographical location and other factors, Xinjiang often suffers from drought. For example, between 1961 and 2000, Xinjiang experienced 17 severe droughts and 9 major droughts (Wen and Shi, 2006). However, Zhang et al. (2012) showed that the drought trend in Different regions of Xinjiang was different, and the drought trend in the western region weakened from 1957 to 2009. Tao, et al. (2014) found that the frequency of extreme drought in the Tarim River basin increased between 1961 and 2010, while Zhang et al. (2015) found that the frequency of drought increased. Most of the previous studies have focused on the historical temporal and spatial changes in

*Abbreviations:* ANN, Artificial neural networks; CMDN, China Meteorological Data Network; ECMWF, European Centre for Medium-Range Weather Forecasts; FED, Frequency of Extreme Drought; FMID, Frequency of Mild Drought; FMOD, Frequency of Moderate Drought; FSD, Frequency of Severe Drought; GD, Global drought; LD, Localized drought; MK, Mann-Kendall; NRX, the Northern Region of Xinjiang; PET, Potential Evapotranspiration; PDSI, Palmer Drought Severity Index; PRD, Partial regional drought; RD, Regional drought; SPEI, Standardized Precipitation Evapotranspiration Index; SPI, Standardized Precipitation Index.

* Corresponding author at: State Key Laboratory of Hydrology-Water Resources and Hydraulic Engineering, Hohai University, Nanjing 210098, China.
*E-mail address:* songjia_hohai@126.com (J. Song).

https://doi.org/10.1016/j.ecolind.2021.107712
Received 15 October 2020; Received in revised form 7 April 2021; Accepted 8 April 2021
Available online 26 April 2021

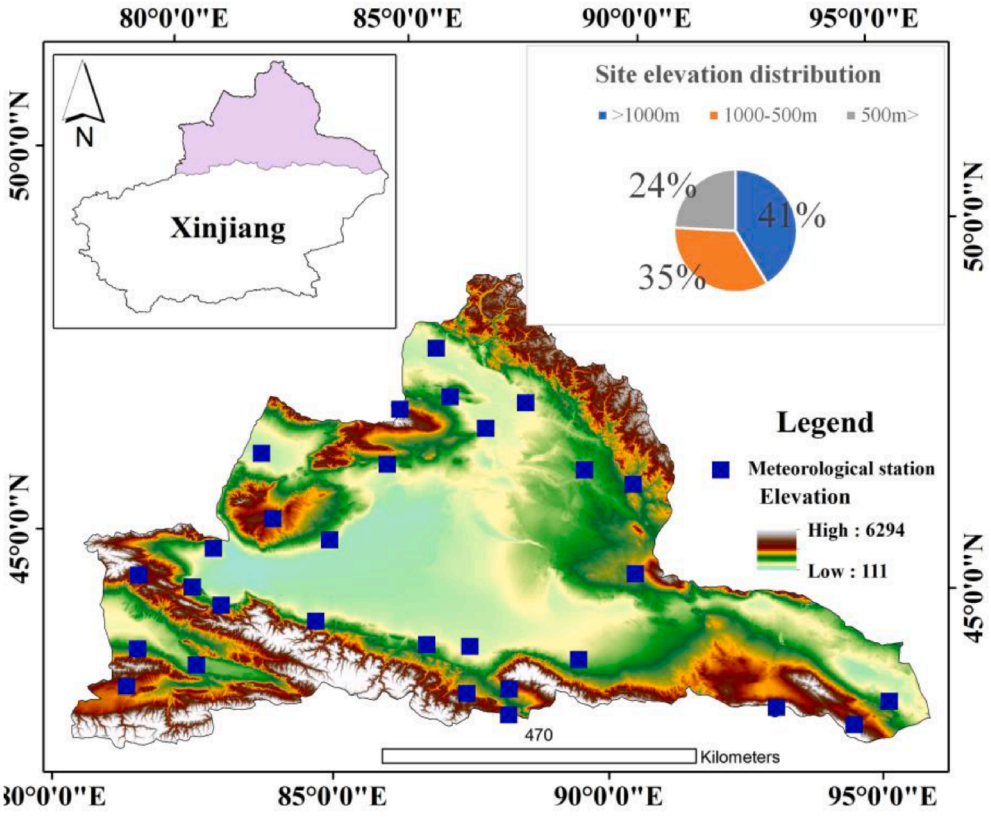


**Fig. 1.** Locations of national meteorological stations in study area mainland.

the context of drought in Xinjiang, but there is still a lack of a comprehensive discussion on drought prediction in Xinjiang. Therefore, we made a comprehensive forecast and assessment of drought conditions in Xinjiang.

At present, to monitor, quantify, describe and evaluate the various indicators of regional drought, scholars at home and abroad have developed hundreds of drought indices (Zargar et al., 2011), such as the PDSI (Liu et al., 2017), SPI and SPEI (Vicente-Serrano et al., 2010a, 2010b). SPI does not consider the impact of evapotranspiration. Therefore, in the context of global warming, it cannot faithfully reflect the impact of temperature changes on drought. As a result, SPI will be biased in assessing the degree of drought (Ci et al., 2016). The SPEI is improved based on the SPI. It uses the interpolation of precipitation on a certain time scale and Based on potential evapotranspiration, combining the advantages of SPI and PDSI indicators to characterize water deficit. It avoids the practical limitations of the SPI index using only a single element (Zhang et al., 2020). At the same time, the SPEI index considers the impact of multi-scale features and meteorological factors such as temperature changes, solar radiation, wind speed, humidity, and altitude on drought. Therefore, it is more advantageous in drought research than the PDSI method that relies on empirical parameters (Chen et al., 2015). So, the SPEI index selected in this paper analyzes the drought situation in NRX.

According to the statistics of the "Chinese Meteorological Disaster Dictionary Xinjiang Volume", the frequency of drought years in northern Xinjiang has reached 36.8%, which is equivalent to a drought year every three years (Wen and Shi, 2006). It can be seen from Fig. s1 (a) that the areas with more precipitation are mainly located in northwestern Xinjiang. Moreover, according to Fig. s1(b), it can be seen that the precipitation in the NRX is decreasing, and the western part of the NRX is showing an increasing trend. The geographical differentiation is obvious, which severely restricts the development of economic in northern Xinjiang. Therefore, people doubt whether the NRX climate change tends to be wet or dry. What is the future trend? This is one of the contents analyzed in this article.

In response to this doubt, this article has designed three main research purposes: (1) modify SPEI based on Thiessen polygon weighting to analyze the drought changes and future trends in NRX from 1960 to 2017. (2) Quantify the scope and extent of drought and the alternating cycles of dry and wet changes. (3) Predict and analyze the dry and wet conditions in the next 5 years based on the ANN. This work has an important guiding role in Xinjiang's development of green agriculture planning.

## 2. Study area

The study area is located in Xinjiang, which is the largest province in Northwest China, with a total area of approximately $44.58 \times 10^4$ km$^2$. Located deep in the arid region of inland China, Xinjiang is a sensitive area of global climate change. Xinjiang's mountains and basins are arranged alternately, and the Tianshan mountains lie in the middle, dividing Xinjiang into southern and northern Xinjiang with very significant climate differences (Zhang et al., 2012; Wang et al., 2014) (Mid-temperate arid zone in northern Xinjiang and warm-temperate arid zone in southern Xinjiang). The study area in this paper belongs to northern Xinjiang (Fig. 1), including many inland rivers. The recharging method is mainly ice and snow meltwater, and rainfall and groundwater recharge are supplemented.

## 3. Materials and methods

### 3.1. Climate data

The daily temperature and precipitation data in this article are derived from the daily data set of China's surface climate data (V3.0) released by the China Meteorological Data Network (CMDN) (http://dat

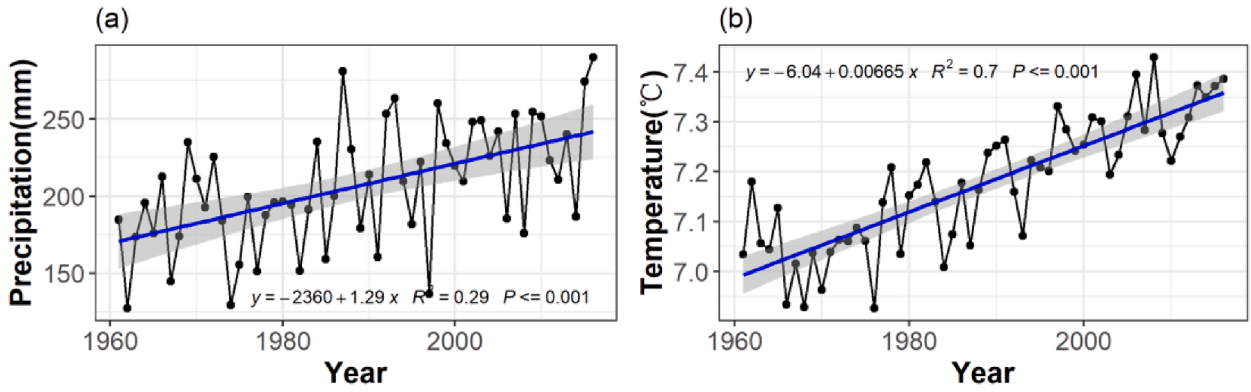


**Fig. 2.** Inter-annual variation of precipitation and surface temperature based on station data (a represents Precipitation (unit: mm); b represents Temperature (unit: ℃)).

a.cma.cn/). Based on the principle of longer period (Yao et al., 2018), the continuity of the data is guaranteed. The stations with discontinuous timing are eliminated, and more stations are retained. Before data processing, the missing data were corrected and interpolated, and stations with more missing measurements in the temperature and precipitation series were eliminated. Moreover, the stations with less missing data were interpolated, and the missing values were interpolated by cubic spline function (An et al.,2020). Consequently, 29 stations with complete and continuous sequence were obtained, as shown in Fig. 1.

Seasonal scale division: Spring includes: March, April, and May; Summer includes: June, July, and August; Autumn includes: September, October, and November; Winter includes: December, January, and February. The gridded precipitation data has a spatial resolution of 1°×1° (Pai et al., 2014) and the gridded temperature data has a spatial resolution of 1°×1° (Srivastava et al., 2009) .

From Fig. 2(b), we can see that from 1960 to 2017, the annual average temperature in northern Xinjiang showed an upward trend, and the temperature fluctuated gently in the late 1960 s, In the mid-1970 s, the upward trend intensified. From 1997 to 2015, the warming trend has been relatively moderate, and this period is now called the "hiatus"(Easterling and Wehner, 2009; Kaufmann et al., 2011). From Fig. 2 (a), it can be seen that the precipitation is in a highly fluctuating upward trend, passing the 99% significance test.

### 3.2. Precipitation data

The selected precipitation data comes from the ERA5 reanalysis data in the European Centre for Medium-Range Weather Forecasts (ECMWF) (www.ecmwf.int). Compared with ERA-Interim, ERA5 assimilated more observation data, the spatial resolution was increased to 0.25°, the temporal resolution was increased to 1 h, and 140 variables were added (Zhao et al., 2019). The spatial resolution is 1°, and the time resolution is the monthly average of 1980–2019.

### 3.3. PDSI data

The PDSI is the first comprehensive drought index developed and is most commonly used to assess the impact of drought on agriculture in the United States. PDSI estimates the drought phase, and considers the precipitation and balance between water supply and demand (including evapotranspiration and soil moisture) (Heim and Richard, 2002). Obtained from KNMI Climate Explorer (http://climexp.knmi.nl/), The spatial resolution is 1°, and the time resolution is the monthly average of 1960–2017.

### 3.4. Methods

#### 3.4.1. SPEI calculation

SPEI has been widely used to monitor drought conditions and one of the important indicators of drought severity and change trends (Tao et al., 2014; Li and Sun, 2017). This index combines the multi-scalar nature of SPI and the sensitivity of PDSI to describe changes in evaporation demand (Vicente-Serrano et al., 2010a, 2010b). So we used SPEI (Vicente-Serrano et al., 2010a) to assess drought variability. Potential Evapotranspiration (PET) is a key factor in calculating SPEI. We use the simplest method to calculate PET (Thornthwaite, 1948). The advantage of this method is that only monthly average temperature data is required. Willmott et al. (1985) modified Thornthwaite's original approach slightly by introducing parameterization for a limited range of average air temperature T (Units: °C): The calculation method of monthly PET (mm) is

$$PET = 0 \quad T < 0$$

$$PET = 16\left(\frac{N}{12}\right)\left(\frac{NDM}{30}\right)\left(\frac{10T}{I}\right)^{m} \tag{1}$$

$$PET = -415.85 + 32.24T - 0.43T^2$$

Where $T$ is the monthly average temperature (°C), $N$ is the maximum solar hours, $NDM$ is the number of days in the month, and $I$ is the heat index. The caloric index is calculated as the sum of the 12 monthly index values $I$: $I$ is derived from the average monthly temperature using formula (2)

$$I = \left(\frac{T}{5}\right)^{1.154} \tag{2}$$

$m$ is calculated from the heat index ($I$) according to the following formula (3)

$$m = 6.75*10^{-7}*I^3 - 7.71*10^{-5}*I^2 + 1.79*10^{-2}*I + 0.492 \tag{3}$$

The following are the SPEI calculation steps: (a) calculate PET;(b) determine the deficit or surplus accumulation of the climate-water balance (Precipitation- Evapotranspiration) on different time scales; (c) normalize the water balance to a logarithmic probability distribution to obtain the SPEI sequence. For a more detailed explanation about the calculation of the SPEI, refer to Vicente-Serrano et al. (2010a).

#### 3.4.2. Thiessen polygon weight calculation

Due to the uneven distribution of meteorological stations, the calculated SPEI index cannot reasonably describe the distribution of drought in the entire region. Therefore, this article first attempts to weight the SPEI data of each station based on the Thiessen polygon area weighting method.

**Table 1**
Grading of the drought impact area.

| Drought station rate | Range Grades |
|---|---|
| 0%~30% | Localized drought (LD) |
| 30%~50% | Partial regional drought (PRD) |
| 50%~70% | Regional drought (RD) |
| 70%~100% | Global drought (GD) |

**Table 2**
Drought frequency classification.

| Drought frequency | Frequency classification |
|---|---|
| 0%~25% | Frequency of Mild Drought (FMID) |
| 25%~50% | Frequency of Moderate Drought (FMOD) |
| 50%~75% | Frequency of Severe Drought (FSD) |
| 75%~100% | Frequency of Extreme Drought (FED)) |

$$\overline{SPEI} = \sum_{i=1}^{n} \frac{S_i}{S} * SPEI_i \tag{4}$$

In the formula: $\overline{SPEI}$is the average SPEI value of a certain time scale in the study area, $n$ is the number of stations, $S_i$ is the Thiessen polygon control area of a certain station, $S$ is the total area of the study area, and $SPEI_i$ is the SPEI value corresponding to a certain station.

The Thiessen polygon converts the point climate index to the area climate index. Compared with the arithmetic average method, it effectively increases the influence weight of sparsely distributed low index points and reduces the influence weight of densely distributed high index points. The result is shown in Fig. s2. The SPEI values of different time scales of the stations in the study area were calculated according to formula (4) to obtain the weighted SPEI time series. The SPEI for all analyses in the study were calculated using weights.

### 3.4.3. Drought station rate calculation

In order to analyze the influence range of different drought degree on different time scale in Xinjiang, this paper selects the drought station rate for quantitative analysis. The calculation formula is:

$$A = \frac{n_1 + n_2 + n_3 + n_4}{N} * 100\% \tag{5}$$

In the formula: $A$ is the ratio of drought stations on a certain time scale, $n_1$, $n_2$, $n_3$, and $n_4$ respectively represent the number of stations with Mild drought, Moderate drought, Severe drought and Extreme drought on a certain time scale, $N$ represents the total number of stations. The comparison table of drought range grades was made according to the drought station ratio (Table 1)

### 3.4.4. Drought frequency calculation

In order to quantify the number of droughts that have occurred in Xinjiang over the years, this study selected drought frequency for quantitative study. The calculation formula is:

$$f = \frac{y}{Y} * 100\% \tag{6}$$

Where: $f$ is the frequency of a certain degree of drought at a certain station on a certain time scale, $y$ is the number of years that a certain station has a certain degree of drought on a certain time scale, and $Y$ is the length of the time series (Potop et al., 2014). We divided the drought frequency into four classifications as shown in Table 2.

### 3.4.5. Trend, MK and Morlet

For a variable $\boldsymbol{y}$ (e.g., SPEI, and PDSI) with a sample size n, a linear regression equation for fitting $\boldsymbol{y}$ versus the year or month index $\boldsymbol{t}$ is given by:

$$\boldsymbol{y} = a\mathrm{t} + b, \mathrm{t} = 1, 2, 3, \cdots, \mathrm{n} \tag{7}$$

where $\boldsymbol{a}$ is the trend slope and $\boldsymbol{b}$ is the y-axis intercept, which can be determined using the least squares method. A positive $\boldsymbol{a}$ value means an increasing trend and a negative value indicates a decreasing trend according to reference (Hu et al., 2015).

Mann-Kendall (M−K) is an effective tool to extract the sequence change trend and has been widely used in the analysis of climate parameters and hydrological sequences (Zhang et al., 2012). It is not affected by a small amount of anomalous data and can be tested to see if the data are mutated. In study, the MK method was chosen to test the trend of the data and the year of the mutation. The calculation formula is as follows:

$$\mathrm{s} = \sum_{i=2}^{n} \sum_{j=1}^{i-1} sign(x_i - x_j) \tag{8}$$

In the formula, sign() is a sign function. When $x_i$ - $x_j$ is less than 0, sign($x_i$- $x_j$) is equal to −1; $x_i$ - $x_j$ is equal to 0, sign($x_i$ - $x_j$) is equal to 0; $x_i$ - $x_j$ is greater than 0, sign ($x_i$ - $x_j$) is equal to 1.

$$z \begin{cases} (s-1)/\sqrt{n(n-1)(2n+5)/18} & S > 0 \\ 0 & S = 0 \\ (s-1)/\sqrt{n(n-1)(2n+5)/18} & S < 0 \end{cases} \tag{9}$$

Where, a positive value of $Z$ indicates an increasing trend, while a negative value indicates a decreasing trend. When the absolute value of $Z$ is greater than or equal to 1.96. It shows that it has passed the 95% significance test of reliability.

The wavelet transform overcomes the disadvantage that the time domain and the frequency domain cannot be taken into account, and the time series can be analyzed from both the time domain and the frequency domain perspectives simultaneously. Morlet wavelets maintain their shape through frequency shifting, which can efficiently separate and reconstruct waves in different frequency bands. There is essentially no loss of time resolution.

In the study, Morlet wavelet is used to analyze the periodicity of SPEI in Xinjiang to determine the future trend. It has good temporal aggregation, high frequency resolution and phase information (Morlet et al., 1982a; Morlet et al.(part i and ii), 1982b). Not only can the fine structure of the SPEI time series be demonstrated, but also the periodic changes that are implied in the sequence over time can also be revealed (Li et al., 2011). The calculation formula is as follows:

A wavelet function is a class of functions that have oscillation characteristics and can decay rapidly to zero . It is defined as:

$$\int_{-\infty}^{+\infty} \phi(t) d_t = 0 \tag{10}$$

Where, φ(t) forms a cluster function system by stretching and shifting: $\phi_{a,b}(t) \in |a|^{-1/2} \phi(\frac{t-b}{a})$,b ∈ R, a ∈ R, a ≠ 0, $\phi_{a,b}(t)$ is a sub-wave; $a$ represents the scale factor, reflecting the cycle length of the wave; $b$ represents the time factor, reflecting the shift in time.

For time series $\phi(t) \in L^2(R)$, $L^2$(R) represents the measurable square product function space defined on the real axis, with its continuous wavelet transformed to:

$$W_f(a,b) = |a|^{-1/2} \int Rf(t) \overline{\phi}(\frac{t-b}{a}) d_t \tag{11}$$

Where, $\overline{\phi}(\frac{t-b}{a})$ is the complex conjugate function of $\phi(\frac{t-b}{a})$; $W_f$ (a,b) is the wavelet transformation coefficient. $W_f$ (a,b) varies with parameters $a$ and $b$, and a two-dimensional contour chart of $W_f$ (a,b) can be made with b as the horizontal coordinates and a as the ordinate. A two-dimensional diagram shows the small wave features of time series changes. The turning point of positive and negative wavelet coefficient corresponds to the mutation point. The greater the absolute value of the wavelet coefficient, the more significant the change of the time scale. The Wavelet Variance is calculated as a formula:

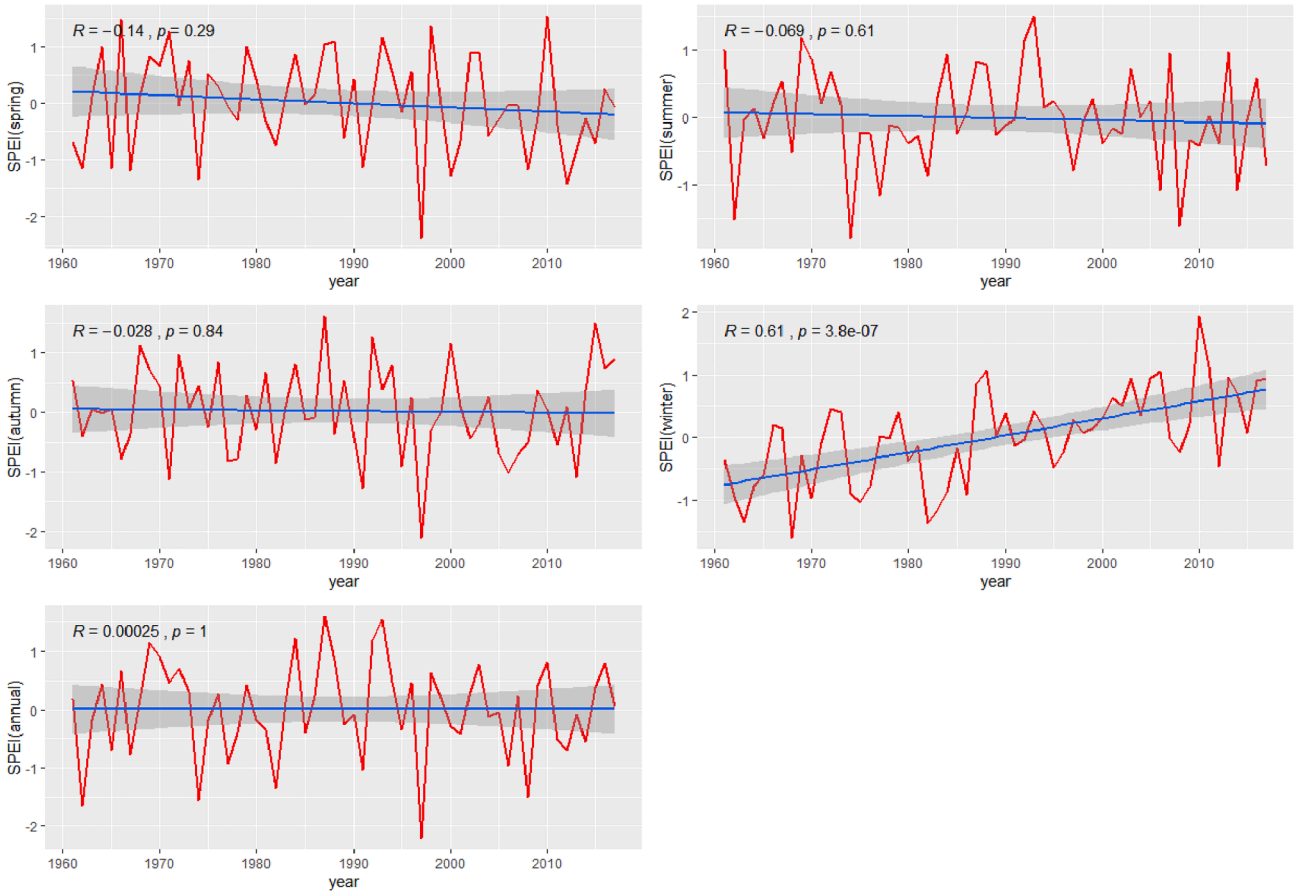


**Fig. 3.** Trend analysis of SPEI index on different time scales.

$$Var(a) = \int_{-\infty}^{+\infty} |W_f(a,b)|^2 db \tag{12}$$

The parameters in the equation refer to (10) and (11). Wavelet Variance can reflect the distribution of energy fluctuations $\alpha$ scale. It can be used to determine the relative strength and main time period of different scale perturbations in the signal. Wavelet Variance enhances the understanding of SPEI's changing cycle and time scale characteristics, and the usage of a wavelet to detect changes in indicator time series gives this research a high improve.

### 3.4.6. Hurst index calculation

Hurst Index (Tong et al., 2018) is mainly used to analyze the future trend of SPEI. When *Hurst* is 0.5, it means that the time series is a random walk, that is, if a place is currently in a drought state, it is not certain whether this state will continue in the future. when $0 \leq Hurst$ less than 0.5, it means that the time series is anti-continuous, that is, if a place is currently in a dry state, the future dry state will gradually ease and tend to be humid. When $0.5 < Hurst \leq 1$, it indicates the positive continuity of the time series. The drought state from the past to the present will continue in the future (Wang et al., 2020).

Consider the *SPEI* (*SPEI*, in the formula, represents variables) time series *SPEI*(t) (t = 1,2,3,4,…,n) for any positive integer $t \geq 1$, define the mean sequence of the time series:

$$\overline{SPEI}_{(\tau)} = \frac{1}{\tau}\sum_{t=1}^{\tau} SPEI_{(\tau)} \tau = 1, 2, \cdots, n \tag{13}$$

Calculate the cumulative dispersion as:

$$X_{(t,\tau)} = \sum_{t=1}^{t} (SPEI_{(t)} - \overline{SPEI}_{(\tau)}) 1 \leqslant t \leqslant \tau \tag{14}$$

The sequence of the Range:

$$R_{(\tau)} = \max_{1 \leqslant t \leqslant \tau} X_{(t,\tau)} - \min_{1 \leqslant t \leqslant \tau} X_{(t,\tau)} \tau = 1, 2, \cdots, n \tag{15}$$

The standard deviation sequence is:

$$S_{(\tau)} = \left[\frac{1}{\tau}\sum_{t=1}^{\tau} (SPEI_{(t)} - SPEI_{(\tau)})^2\right]^{\frac{1}{2}} \tau = 1, 2, \cdots, n \tag{16}$$

Calculate the Hurst index:

$$\frac{R_{(\tau)}}{S_{(\tau)}} = (c\tau)^H \tag{17}$$

In the formula, $c$ is a constant. The Hurst empirical formula is obtained by taking the logarithm of both sides of the method (17). Based on time series and using Hurst's practical method to get a cluster of $H$ values for least-squares fitting, the straight-line slope obtained is the modified Hurst index ($H$), which reveals the fractal characteristics of the time series.

**Table 3**
Mutation year of SPEI at different time scales.

| Time Scale | Mutation time (years) | Significant (Yes or No) |
|---|---|---|
| Spring | 2000, 2004 | No |
| Summer | 1960, 1963, 1974, 1982, 2005, 2007, 2013, 2015, 2016 | No |
| Autumn | 1960 ~ 1967, 1977 ~ 1978, 1982, 1988 ~ 1989, 1991 ~ 1992, 2016 | No |
| Winter | 1994 | Yes |
| Annual | 1962, 1981, 1996, 1998, 2000, 2002, 2014, | No |

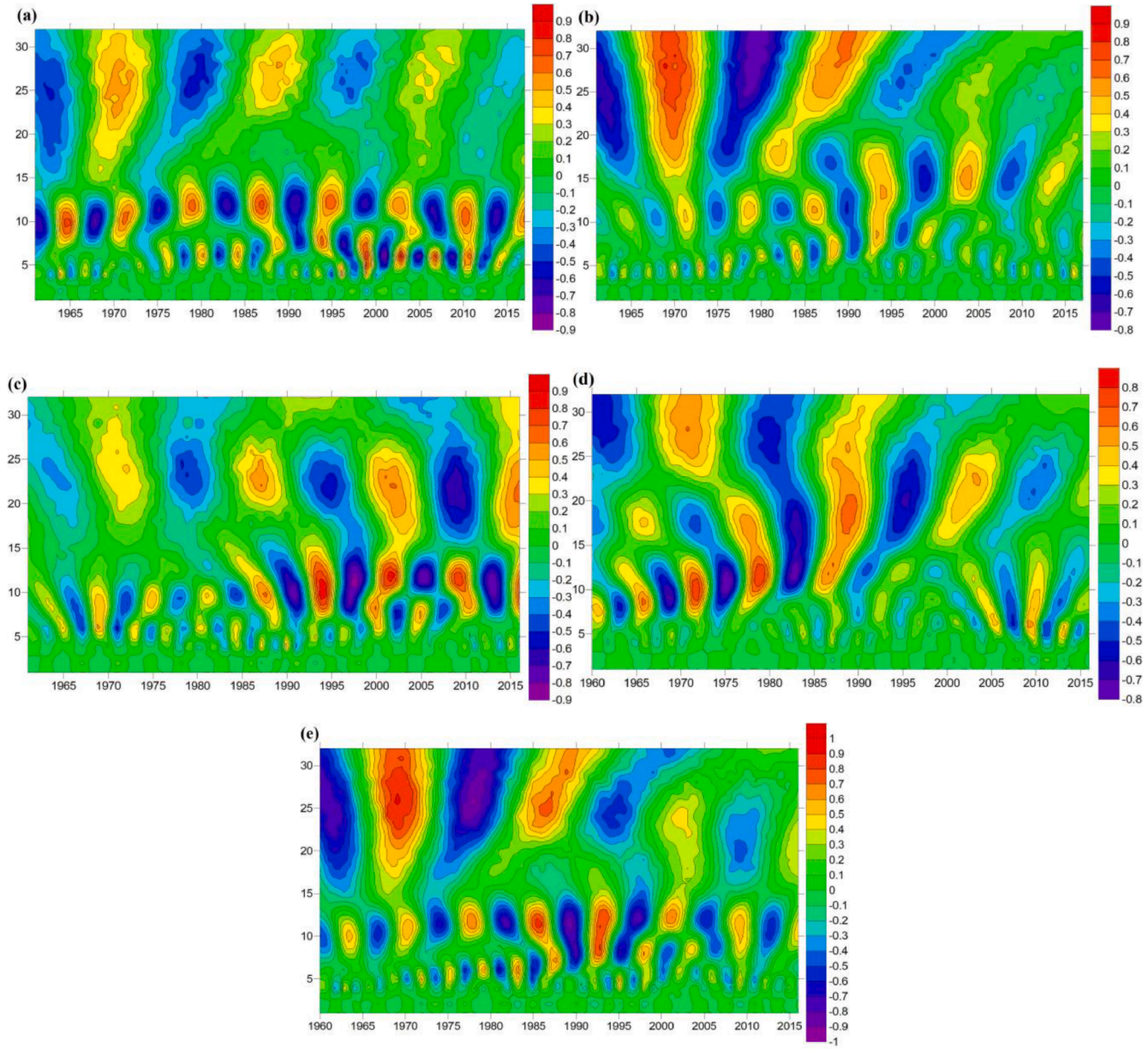


**Fig. 4.** SPEI time-series change characteristics analysis based on wavelet analysis ((a): spring; (b): summer; (c); autumn; (d): winter; (e): annual; Red indicates a high value, indicating wetting, and Blue indicates a low value, indicating dry). (For interpretation of the references to colour in this figure legend, the reader is referred to the web version of this article.)

### *3.4.7. A multi-layer feed-forward network*

Artificial neural networks are forecasting methods based on simple mathematical models of the brain. They allow complex nonlinear relationships between the response variable and its predictors (Chen et al., 2020). A neural network can be thought of as a network of "neurons" which are organized in layers. The predictors (or inputs) form the bottom layer, and the forecasts (or outputs) form the top layer. There may also be intermediate layers containing "hidden neurons".

This is known as a multilayer feed-forward network, where each layer of nodes receives inputs from the previous layers. The outputs of the nodes in one layer are inputs to the next layer. The inputs to each node are combined using a weighted linear combination. The result is then modified by a nonlinear function before being output. For example, the inputs into hidden neuron *j* in Fig. s3 are combined linearly to give the input for the next layer.

$$z_j = b_j + \sum_{i=1}^{4} w_{i,j} x_i \tag{18}$$

In the hidden layer, this is then modified using a nonlinear function such as a sigmoid, the transfer and output functions in the hidden layer are *Tan-sigmoid*. The hidden layer parameters of this study are: weights (ω) and threshold (*z*) information on the association of layer and layer neuron nodes, They need to be acquired through continuous learning and training of the network.

$$s(z) = \frac{i}{1 + e^{-z}} \tag{19}$$

This tends to reduce the effect of extreme input values, thus making the network somewhat robust to outliers. The parameters *b1*, *b2*, *b3*, and *w1,1*, …, *w4,3*, are "learned" from the data. The values of the weights are often restricted to prevent them from becoming too large. The parameter that restricts the weights is known as the "decay parameter", and is often

**Table 4**
SPEI change characteristics of different time series scales.

| Time Scale | First main cycle (year) | Number of oscillation (First main cycle) | Second main cycle (years) | Number of oscillations (Second main cycle) | Third main cycle (years) | Number of oscillations (Third main cycle) |
|---|---|---|---|---|---|---|
| Spring | 11 | 8 | 6 | 8 | 26 | 4 |
| Summer | 28 | 3 | 17 | 5 | 4 | 16 |
| Autumn | 11 | 8 | 22 | 4 | 6 | 14 |
| Winter | 11 | 8 | 18 | 5 | 25 | 4 |
| Annual | 25 or 26 | 4 | 12 | 8 | 6 | 14 |

set to be equal to 0.1.

The weights take random values, to begin with, and these are then updated using the observed data. Consequently, there is an element of randomness in the predictions produced by a neural network. Therefore, the network is usually trained several times using different random starting points, and the results are averaged. The detailed process of the model construction process is as follows: (1) data standardization: the input data units are different; (2) determine the hidden layer and hidden nodes of the network; (3) design the prediction year and select the training function.

## 4. Results and analysis

### 4.1. Trend analysis of SPEI

The weighted SPEI index of different time scales from 1960 to 2017 was subjected to linear regression to analyze the changing trend of the SPEI index in NRX in the past 57 years. The trend graph is shown in Fig. 3. It can be seen from the linear trend graph that the SPEI index in spring, summer, and autumn all declined at a slow rate, and the correlation coefficient did not pass the significance test of $\alpha = 0.05$, indicating that although the SPEI has tended to be arid in the past 57 years, the trend is not significant. In the spring of 1997, the minimum SPEI was −2.37, which was an extreme drought; In the summer of 1974, the minimum SPEI was −1.78, which was a severe drought; In the autumn of 1997, the minimum SPEI was −2.11, which was an extreme drought; Winter SPEI increases at a rate of 0.027/year, and the correlation coefficient $R = 0.61 > r_{0.01} = 0.3415$, indicating that the increase in winter SPEI over the past 57 years is significant with 99% confidence.

The main reason for the warm and humid winters and the lack of significant changes in the rest of the season in NRX is the fact that the most significant increase in precipitation over the past half-century occurred mainly in NRX (Yao et al.,2018). It has been shown that winter temperatures in the arid northwest have been growing up over the past 50 years (Li et al., 2012). Studies of temperature variation across seasons have shown that winter mean temperature contributes 57.01% to the rate of increase in annual mean temperature (Chen et al., 2015). Therefore, the significant increase in winter temperature may be an important reason for the risein mean annual temperature in the NRX.

### 4.2. SPEI Mann-Kendall inspection

To further determine the change trend and mutation points of the SPEI sequence, the Mann-Kendall mutation test were performed on the SPEI time series at different time scales. In addition, we used the significance level of 0.05, as shown in Table 3.

**Table 5**
R/S analysis table for SPEI 1960–2017.

| Time | Regression Equations | $R^2$ | Hurst |
|---|---|---|---|
| Spring | y = -0.0753 + 0.517x | 0.99 | 0.517 |
| Summer | y = -0.123 + 0.582x | 1 | 0.582 |
| Autumn | y = -0.0365 + 0.5x | 0.99 | 0.5 |
| Winter | y = -0.0776 + 0.546x | 1 | 0.546 |
| Annual | y = -0.105 + 0.57x | 0.98 | 0.57 |

From the results of SPEI's MK mutation test on different time scales. In spring, summer, autumn and annual , they did not pass the 0.05 confidence level test (Fig. s4), and the variation was not very variable.

The rising trend of the UF curve is relatively obvious. Only 1960–1964 and 1985 were in a drought trend, and the rest of the period were in a humid trend. After 1987, this humidification trend exceeded the significance level of 0.05 line in Winter (Table 3 and Fig. s4). It shows that in the past 57 years, the trend of winter wetness in NRX was obviously significant. In terms of different seasons, only winter is the most significant, and the trend of SPEI in winter is generally consistent with previous studies (Shi et al., 2003; Chen et al., 2011). In the past 50 years, the climate in the western Tianshan region of Xinjiang had shown a warm and humid direction (Shi et al., 2003), which is consistent with the results of winter changes (Fig. 3). As it can be inferred that the change from drought to wetness in Xinjiang over the past 50 years is mainly due to changes in winter temperature and precipitation (Yang et al., 2012). However, the winter SPEI showed a dramatic increase in variation from 1987. There is no evidence of to what causes it (Chen and Xu. 2004).

### 4.3. Morlet wavelet analysis of SPEI

To explore the regularity of the SPEI index in NRX, we perform Morlet continuous wavelet transformation on the weighted SPEI index sequence of different time scales in the past 57 years and finally get the wavelet real part contour map and wavelet variance map of different time (Fig. 4). On the left is the contour map of the real part of the wavelet for each time scale. The higher the value, the more humid, and the lower the value, the drier; The periodic characteristic analysis results of wavelet analysis are shown in Table 4.

From Fig. 4 and Table 4, we can see that the wavelet coefficients exhibit a three-major-period variation pattern across seasons (contour plots, SPEI greater than 0, indicating wetness; SPEI less than 0, indicating drought). In particular, spring, summer, autumn, winter and annual average scale all show obvious changes in the three main cycles, and show a clear pattern of alternating oscillations of drought and wetness, and are global in nature. The different time scales are also accompanied by multiple small-period oscillations, but more turbulent.

Combined with the wavelet variance plot (Fig. s5), there are two peaks in spring. The 11th year is highest and the largest, the 28th year is the highest and largest in the summer, the 11th year is the largest in the fall, the 11th year is the largest in the winter, and the 25th and 26th years are the largest annual increase. The period with the strongest annual SPEI vibration was diagnosed as 8 year in NRX, it result is consistent with the research results of precipitation cycle fluctuation in western China (Guo et al., 2013). Thus, it can be concluded that the annual main cycle of SPEI in northern Xinjiang is mainly influenced by the summer main cycle.

In addition, we can also predict the drought situation in the future based on the result of the wavelet real part contour. The spring of 2017 was in a humid state, while in summer, autumn and winter, the annual average scale was in a wet and dry state. According to the drought and humid conditions in 2017, taking the year of the first main cycle as the oscillation period, it can be seen that there may be a dry state in the spring of 2021, It may change to a humid state in the summer, autumn,

**Table 6**
Comparison table of drought years.

| Time Scale | Total Number of years | LD Number of years | PRD Number of years | RD Number of years | GD Number of years |
|---|---|---|---|---|---|
| Spring | 57 | 10 | 11 | 5 | 10 |
| Summer | 57 | 13 | 23 | 4 | 5 |
| Autumn | 56 | 13 | 12 | 8 | 6 |
| Winter | 57 | 22 | 8 | 5 | 10 |
| Annual | 56 | 18 | 9 | 5 | 9 |

winter and average annual scale. In light of this we can deduce that there is a greater chance of shifting from drought to humid at different time scales in NRX.

### 4.4. *The future trend of SPEI*

To further verify the reliability of the SPEI development trend predicted by the wavelet, we performed the Hurst index method calculation based on the *R/S* analysis method on the SPEI series of different time scales in northern Xinjiang and compared the results obtained with the


**Fig. 5.** The proportion of drought sites in different impact ranges ((a): spring; (b): summer; (c); autumn; (d): winter; (e): annual).

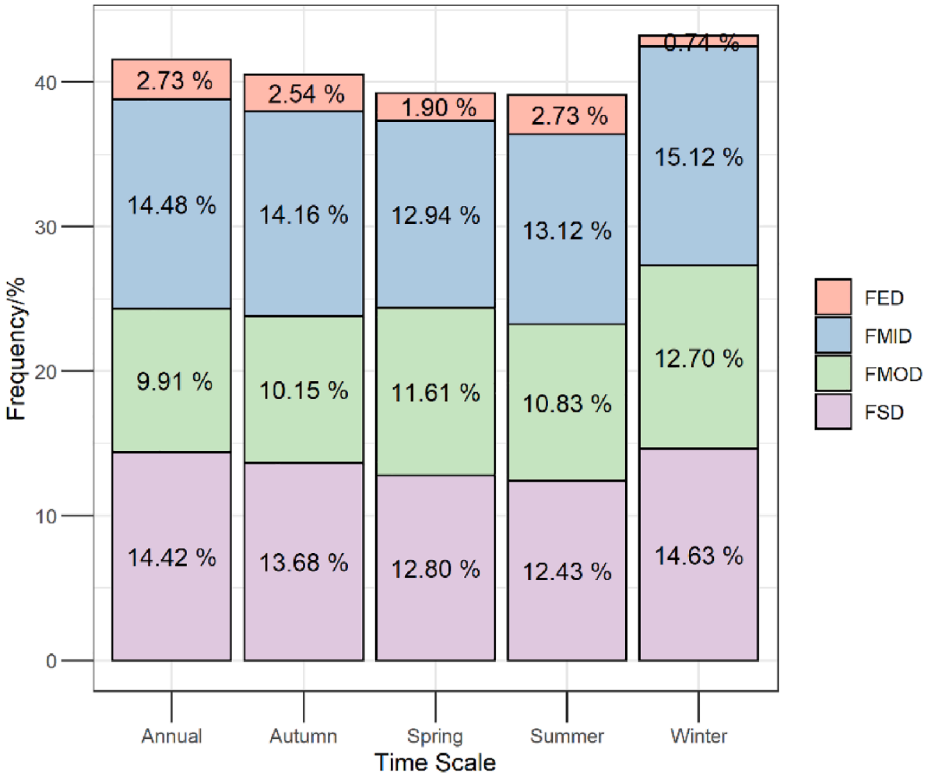


**Fig. 6.** Drought frequency distribution at different time scales.

results of the wavelet prediction. The result of the Hurst exponent operation is shown in Table 5.

It can be seen from the results of the bar chart in Table 6 that The Hurst index of SPEI in spring, summer, winter, and annual scales is greater than 0.5, indicating that the SPEI index will continue the original trend. The unary linear regression trend in autumn in Fig. 3 shows that in the future spring and summer will continue to be dry, winter will continue to be humid, and the annual scale will continue to be humid. The results are consistent with the prediction results on different main periods of wavelet analysis (Fig. 4).

### 4.5. The status of drought range in different time scales

To clarify the impact of drought on different time scales in NRX, according to the classification of drought levels in Table 1, we classify and count the number of stations with different degrees of drought each year at different scales, and obtain different levels of drought each year at different scales. The ratio of drought stations is shown in Fig. 5. We classify and count the number of drought stations per year according to Table 2, and the final results are shown in Table 6.

It can be seen from Fig. 5 (a) and Table 6: Firstly, The number of spring drought years is 36 years, accounting for only 63.2% of the total number of years, indicating that the probability of spring drought in northern Xinjiang is over 60% each year. Some regional droughts have occurred with the largest proportion of years (19.3%). Secondly, The ratio of drought stations in summer varies from 0% to 93.1%. Some regional droughts occurd with the largest proportion of years (40.4%). LD occurred in autumn, which accounted for the largest proportion (23.2%). LD occured in winter, which accounted for the largest proportion (23.2%); LD occurred on an annual scale with the largest proportion (32.1%).

In summary, the spring regional droughts in NRX are prone to occur; PRD is more likely to occur in summer. LD and PRD are more likely to occur in autumn. LD is more likely to occur in winter; mainly Mild droughts and Moderate droughts. The annual-scale LD has a great chance of occurring.

### 4.6. Drought frequency in different time scales

To clarify the frequency of droughts at different time scales in the NRX, the frequency of droughts of different levels in all stations was counted, and the result of drought frequency was finally shown in Fig. 6.

Obtained from Fig. 6, the FMID is the largest in spring, summer, autumn, winter, and annual-year at various sites in NRX, respectively: 12.97%, 13.12%, 14.16%, 15.12%, and 14.48%. Generally speaking, the FMID is the greatest and the probability of occurrence has increased. In other words, the greater the chance of FMID, the greater the chance of becoming wet. It can be seen from Fig. 6 that the FMID is the largest in spring, summer, autumn, winter, and annual-year at various sites in NRX, respectively: 12.97%, 13.12%, 14.16%, 15.12%, and 14.48%. The FSD was 12.8%, 12.43%, 13.68%, 14.63% and 14.42%. Generally speaking, the probability of a mild drought is the greatest and the probability of occurrence has increased. In other words, the greater the chance of mild drought, the greater the chance of becoming wet.

### 4.7. Predictive analysis of arid climate

#### 4.7.1. Drought history

In the context of global warming, the study of drought issues no longer focuses on precipitation, and the influence of temperature-related to evaporation on drought trends is becoming more and more significant (Chen and Sun, 2015). Since the 1960 s, Xinjiang's warming trend has been significant, which has led to increased evaporation and frequent droughts. However, the temperature increase in winter in NRX is also obvious, with a temperature increase rate of 0.34℃/10a (Zhang et al., 2019). According to the linear regression trend of the SPEI (Fig. 3-

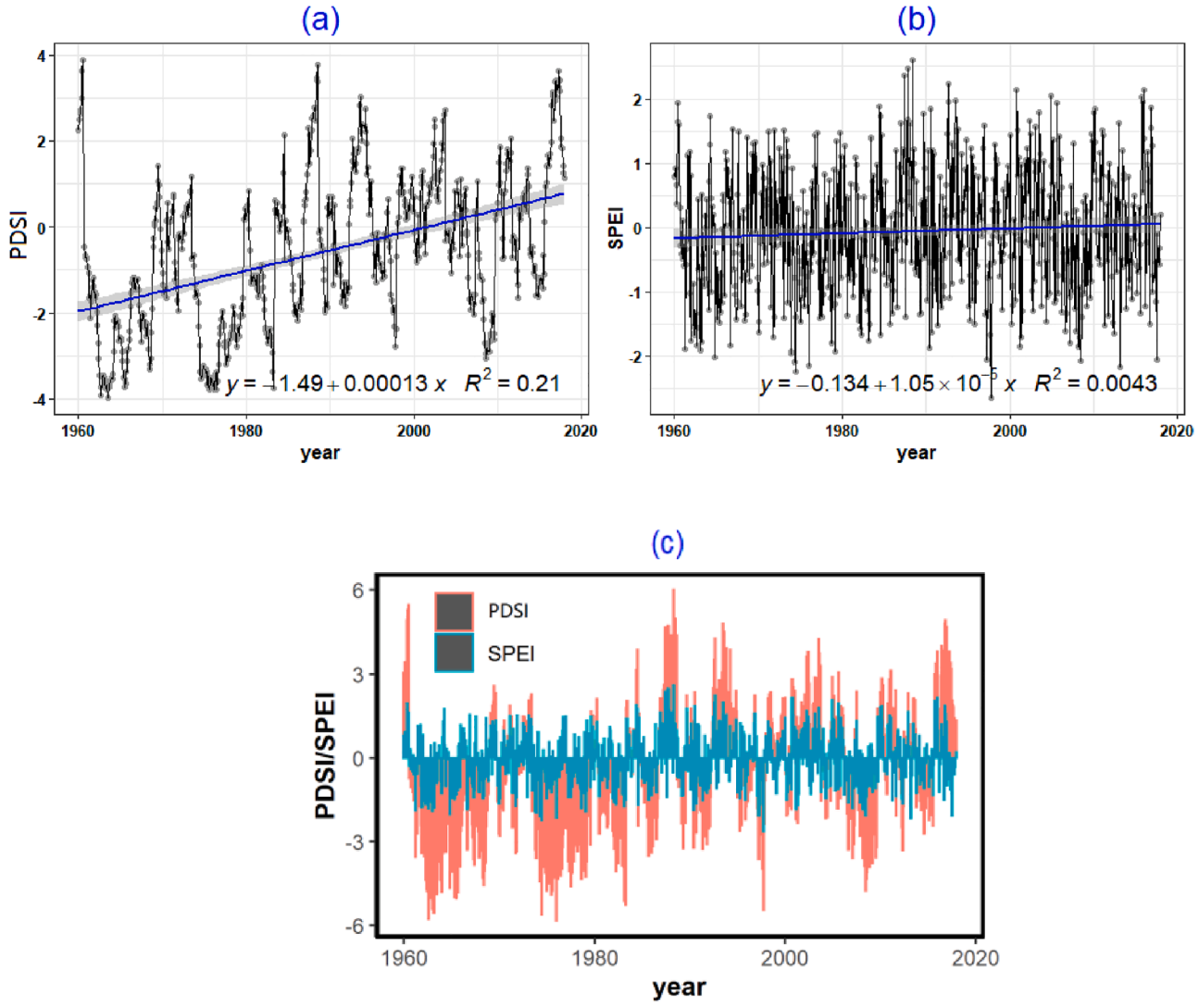


**Fig. 7.** Analysis of drought index changes in the historical period.

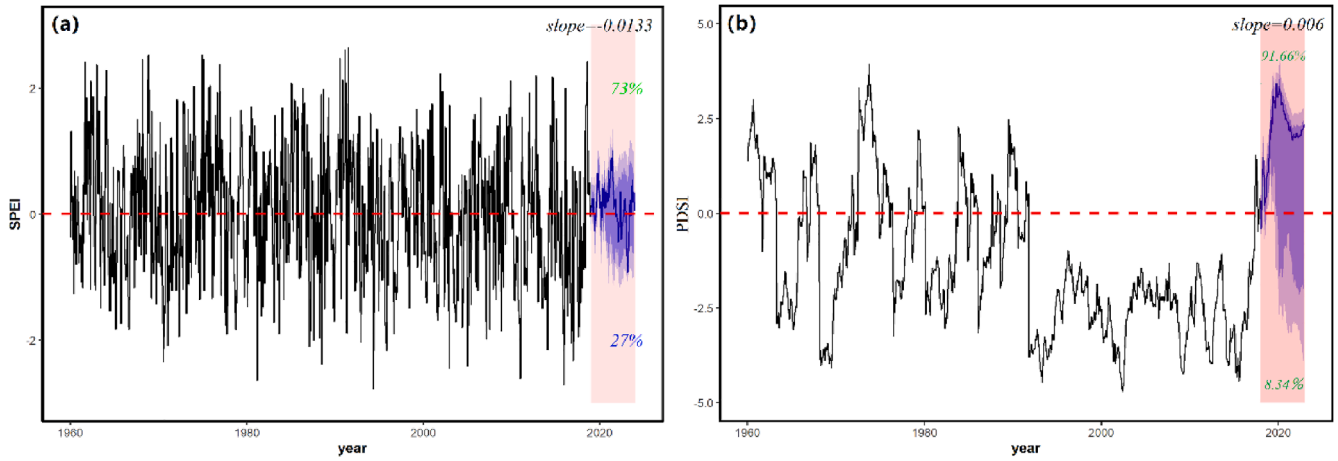


**Fig. 8.** Analysis of changes in the forecast of drought index (**Black line** represents the monthly change trend of the drought index; **Red dotted line** represents drought index equal 0; **the Blue line** represents the predicted change trend, **the Blue area** represents the 95% confidence interval; **Slope** represents the slope of the predicted drought index; **Percentage** represents the proportion of dry months in total months (forecast month)). (For interpretation of the references to colour in this figure legend, the reader is referred to the web version of this article.)

winter), however, we found that winter shows a trend of humidification. In recent years, the Arctic Oscillation has been negative for many years, which has caused the high pressure to move northward and the cold air can move southward, resulting in lower temperatures and increased extreme snowfall in NRX. As a result, there is a trend of humidification in NRX. Therefore, we selected SPEI and PDSI to consider the influence of temperature to conduct comparative analysis and prediction of drought conditions.

To reduce the uncertainty of the data, the PSDI is also selected for comparison simulation prediction. Firstly, the SPEI data of the site is spatially interpolated to make a resolution of 1° to ensure the same resolution of the PDSI data. Then the changing trends and spatial distribution are compared and analyzed.

According to Fig. 7(a), the PDSI has shown a significant upward trend in the historical period, indicating that the degree of drought is decreasing, the slope of change is 0.00013/a and $R^2$ is equal to 0.21. From 1960 to 2017, the PDSI changed dramatically. And the PDSI was negative before 1990, indicating that drought occurred more frequently before 1990. According to Fig. s6(b), most areas in the PDSI space show an upward trend, and the eastern part has a downward trend. From Fig. s6(d), it can be seen that the PDSI in most of the NRX is negative, indicating that most of the NRX is an arid area, but the degree of drought is decreasing. In the past 60 years, the annual precipitation in NRX has generally shown a significant increase trend which is consistent with the change trend of PDSI (He et al. 2020), because the water supply and demand considered by PDIS are usually replaced by precipitation.

Secondly, it can be seen from the change trend of the SPEI index in Fig. 7(b) that the SPEI index shows a rising trend but not significant, the change slope is −0.0000105, the $R^2$ is equal to 0.0043. PDSI considers the current water supply and demand situation: including soil moisture, land use, and soil texture, etc. The change trend of PDSI indirectly indicates the loss of soil moisture but no increase in evaporation (Li et al., 2017). The difference between standardization of potential evapotranspiration and precipitation was used to characterize the degree of deviation of drought conditions. Therefore, the historical period of SPEI has a smaller range of changes compared to PDSI. From Fig. s6(a), the SPEI has changed from dry to humid in the western and northern parts of the NRX. The degree of drought in the eastern region is deepening. From Fig. s6(c), the spatial distribution of dry and wet conditions is humid in the north and west and dry in the east of the NRX.

#### 4.7.2. Drought future

The future trend of dry and wet climate in NRX was further proved. On the basis of the neural network model, the degree of drought in the next 5 years (2018–2022 month scale) are predicted. From Fig. 8(a), it can be seen that the SPEI model prediction results are as follows: from 1960 to 2017, the range of SPEI changes is large and there is no obvious pattern. The predicted change slope of SPEI is −0.0133/*month* from 2018 to 2022, indicating that the predicted SPEI will show a downward trend in the next 5 years. However, from the statistical forecast of SPEI, months greater than 0 (representing wet) account for 73% of the total forecast months. It shows that the wet months are predicted to account for most of them within 5 years; Months less than 0 (representing drought) account for 27% of the total forecast months. Overall, based on the neural network model's prediction of SPEI in the next 5 years, there is a greater chance of a humid climate.

From Fig. 8(b), the PDSI increased significantly from 1960 to 2017 due to precipitation (Zhang et al., 2013). The wet months accounted for 91.66% of the total forecast months, and the dry months accounted for 8.34% in the next 5 years. And it shows an upward trend, the slope of change slope is equal to 0.006/*month*. In general, according to the prediction results of the neural network model, the NRX of Xinjiang will show a trend of humidification in the next 5 years and the probability is relatively high.

### 4.8. Discussion

Climate change is undoubtedly complex in the arid northwest China. In the short term, it is difficult to accurately reveal the process and trend of its change. Many studies focus on the analysis of climate characteristics on different time scales at regional scale. However, most of these studies are qualitative descriptions and lack of quantitative data.

The increase in temperature, the increase in evaporation, and the serious loss of soil moisture led to increased drought in Xinjiang (Li and Sun, 2017). However, according to Fig. 2 (a) and (b), it can be seen that precipitation has increased in northern Xinjiang, the temperature has risen, and the climate has changed towards warm and humid.

At the beginning of the 21st century, Shi et al, (2003) put forward the view that the climate in northwest China will transition from warm and dry to warm and humid, which has been confirmed by all parties. After 2000, the area rate of extreme drought has increased (Jiang and Hu, 2004), especially in northern Xinjiang and Tianshan Mountains (Li and Jiang, 2007; Li et al., 2017). The evolution of natural climate indicates that it may enter a period of low precipitation in multiple decades, which will complicate the precipitation change scenarios in specific regions and periods in the future. According to the findings of Zhang et al. (Zhang et al., 2012), the assessment of the severity of drought in Xinjiang has declined in recent years. However, it only analyzes the intensity and frequency of drought based on precipitation and temperature, and does not consider the impact of continuous no-precipitation days and soil moisture on drought. Therefore, wet and dry conditions may not be a real phenomenon. Therefore, there is a lot of uncertainty in the future prediction.

Therefore, in future research, this article believes that it is necessary to understand how the climate change mechanism affects the water cycle and water system, or emphasize the need to further understand the different time scales of the evolution of the climate system and their interaction rules to better predict the future dry and wet conditions.

## 5. Conclusions

In this study, the daily precipitation and temperature data of 29 stations in NRX from 1960 to 2017 were used to calculate the PET using the Thornthwaite method. Then the SPEI of different time scales in the NRX was calculated. For the problem of uneven spatial distribution, the SPEI is weighted by the area of the Thiessen polygon method. It's an attempt for Xinjiang's complex terrain. In winter, the trend toward humidification is significant, and the trend of the SPEI series tested by MK is relatively stable. Based on the wavelet transform, we roughly infer the increasing trend of wetting that may occur under different time scales at NRX in 2021. The results of the Hurst index show that: winter and annual scales will continue to be humidified, and spring, summer, and autumn will continue to be arid.

In the spring and summer of NRX, LSD is more likely to occur. According to the results obtained from the analysis of drought frequency, the average frequency of droughts on various time scales in NRX is above 30%. In other words, droughts in NRX occur at least once every three years, which is a high frequency. According to the predicted results, the probability of future regional humidification is high in NRX.

## Declaration of Competing Interest

The authors declare that they have no known competing financial interests or personal relationships that could have appeared to influence the work reported in this paper.

## Acknowledgments

The research was carried out with the financial support provided by the Strategic Priority Program of the Chinese Academy of Science (CAS), PanThird Pole Environment Study for a Green Silk Road

(XDA20040400) The authors wish to thank the referees for providing helpful suggestions to improve this manuscript. Thanks the graduate student Wu Xiu Yi and Li Jun for providing language helpful to improve this manuscript .

## Appendix A. Supplementary data

Supplementary data to this article can be found online at https://doi.org/10.1016/j.ecolind.2021.107712.

## References


An, Q., He, H., Gao, J., Nie, Q., Xie, X., 2020. Analysis of temporal-spatial variation characteristics of drought: A case study from Xinjiang, China. Water 12 (3), 741. https://doi.org/10.3390/w12030741.

Chen, F., Yuan, Y., Wen, W., Yu, S., Shang, H., 2011. Tree-ring-based reconstruction of precipitation in the changling mountains, China, since a.d.1691. Int. J. Biometeorol. 56 (4), 765–774.

Chen, H., Sun, J., 2015. Changes in drought characteristics over China using the standardized precipitation evapotranspiration index. J. Clim. 28 (13), 5430–5447.

Chen, Y., Li, Z., Fan, Y., Wang, H., Deng, H., 2015. Progress and prospects of climate change impacts on hydrology in the arid region of northwest china. Environ. Res. 139 https://doi.org/10.1016/j.envres.2014.12.029.

Chen, Y.N., Xu, Z.X., 2004. The possible impact of global climate change on water resources in the Tarim River Basin. Sci. China Ser. D 34 (11), 1047–1053.

Chen, Y.N., Yao, Q., Li, Y., Yan, J.S., Xiang, L.P., Lan, H.L., 2012. Ponder on the issues of water resources in the arid region of northwest China. Arid Land Geography 35 (1), 1–9.

Chen, X.F., Leeuw, G.D., Anola, A., Liu, S.M., Liu, Y., Li, Z.Q., et al. 2020. Joint retrieval of the aerosol fine mode fraction and optical depth using MODIS spectral reflectance over northern and eastern China: Artificial neural network method. Rem. Sens. Environ. 249. https://dx.doi.org/10.1016/j.rse.2020.112006.

Ci, H., Zhang, Q., Xiao, M.Z., 2016. Evaluation and comparability of four meteorological drought. Acta Scientiarum Naturalium Universitatis Sunyatseni 55 (02), 124–133.

Dai, A., 2013. Increasing drought under global warming in observations and models. Nat. Clim. Change 3 (1), 52–58.

Dubrovsky, M., Svoboda, M.D., Trnka, M., Hayes, M.J., Wilhite, D.A., Zalud, Z., Hlavinka, P., 2009. Application of relative drought indices in assessing climate-change impacts on drought conditions in Czechia. Theor. Appl. Climatol. 96 (1–2), 155–171.

Easterling, D.R., Wehner, M., 2009. Is the climate warming or cooling? Geophys. Res. Lett. 36 (8) https://doi.org/10.1029/2009GL037810.

Guo, H., Li, D.L., Lin, S., Dong, Y.X., Sun, L.D., Huang, L.N., 2013. Temporal and spatial variation of precipitation over western China during 1964–2006. J. Glaciol. Geocryol. 35 (5), 1165–1175.

He, B.B., Sheng, Y., Cao, W., Wu, J.C., 2020. Characteristics of Climate Change in Northern Xinjiang in 1960–2017, China. Chin. Geogr. Sci. 30 (02), 63–79.

Heim, Richard, R., 2002. A review of twentieth-century drought indices used in the United States. Arid Meteorol. 24 (1), 79–89.

Hu, Q., Pan, F.F., Pan, X.B., Zhang, D., Li, Q.Y., Pan, Z.H., et al., 2015. Spatial analysis of climate change in Inner Mongolia during 1960–2012, China. Appl. Geogr. 60, 254–260.

Jiang, F.Q., Hu, R.J., 2004. Climate change and flood & drought disasters in Xinjiang during recent 50 years. J. Desert Res. 24 (1), 35–40.

Kaufmann, R.K., Kauppi, H., Mann, M.L., Stock, J.H., 2011. Reconciling anthropogenic climate change with observed temperature 1998–2008. Scholarly Articles 108 (29), 11790–11793.

Liu, Y., Zhang, X., Song, H., Cai, Q.F., Li, Q., Zhao, B.Y., et al., 2017. Tree-ring-width-based PDSI reconstruction for central Inner Mongolia, China over the past 333 years. Clim. Dyn. 48 (3), 867–879.

Li, B., Chen, Y., Shi, X., 2012. Why does the temperature rise faster in the arid region of northwest China? J. Geophys. Res. Atmos. 117 (D16) https://doi.org/10.1029/2012JD017953.

Li, Z., Jiang, F.Q., 2007. A study of abrupt climate change in Xinjiang region during 1960–2004. J. Glaciol. Geocryol. 29 (3), 351–359.

Li, Y., Sun, C., 2017. Impacts of the superimposed climate trends on droughts over 1960–2013 in Xinjiang, China. Theor. Appl. Climatol. 977–994.

Li, Y., Yao, N., Sahin, S., Appels, W.M., 2017. Spatiotemporal variability of four precipitation-based drought indices in xinjiang, china. Theor. Appl. Climatol. 129 (3–4), 1017–1034.

Li, M., Xia, J., Chen, S.M., Meng, D.J., 2011. Wavelet analysis on annual precipitation around 300 years in Beijing Area. J. Nat. Res. 26 (6), 1001–1011.

Morlet, J., Arens, G., Fourgeau, E., Giard, D. 1982. Wave propagation and sampling theory; Part i, complex signal and scattering in multilayered media. Geophysics. 1982, 47(2):203–221.

Morlet, J., Arens, G., Fourgeau, E., Giard, D., 1982b. Wave propagation and sampling theory; Part II, sampling theory and complex waves. Geophysics 47 (2), 222–236.

Pai, D., Sridhar, L., Rajeevan, M., Sreejith, O., Satbhai, N., Mukhopadhyay, B., 2014. Development of a new high spatial resolution (0.25 × 0.25) long period (1901–2010) daily gridded rainfall data set over India and its comparison with existing data sets over the region. Mausam 65(1):1–18.

Potop, V., Boroneant, C., Mozny, M., Stepanek, P., Skalak, P., 2014. Observed spatiotemporal characteristics of drought on various time scales over the Czech Republic. Theor. Appl. Climatol. 115 (3), 563–581.

Shi, Y.F., Shen, Y.P., Li, D.L., Zhang, G.W., Ding, Y.J., Hu, R.J., 2003. Discussion on the present climate change from warm–dry to warm–wet in Northwest China. Quat. Sci. 23 (2), 152–164.

Srivastava, A., Rajeevan, M., Kshirsagar, S., 2009. Development of a high resolution daily gridded temperature data set (1969–2005) for the Indian region. Atmos. Sci. Lett. 10 (4), 249–254.

Tao, H., Borth, H., Fraedrich, K., Su, B., Zhu, X., 2014. Drought and wetness variability in the Tarim River Basin and connection to large-scale atmospheric circulation. Int. J. Climatol. 34 (8), 2678–2684.

Thornthwaite, C.W., 1948. An approach toward a rational classification of climate. Geogr. Rev. 38 (1), 55–94.

Tong, S., Lai, Q., Zhang, J., Bao, Y., Lusi, A., Ma, Q., et al., 2018. Spatiotemporal drought variability on the Mongolian Plateau from 1980–2014 based on the SPEI-PM, intensity analysis and Hurst exponent. Sci. Total Environ. 615, 1557–1565.

Vicente-Serrano, S.M., Beguería, S., López- Moreno, J.I., 2010a. A multiscalar drought index sensitive to global warming: The standardized precipitation evapotranspiration index. J. Clim. 23 (7), 1696–1718.

Vicente-Serrano, S.M., Begueria, S., Lopezmoreno, J.I., 2010b. A New Global 0.5° Gridded Dataset (1901–2006) of a multiscalar drought index: Comparison with current drought index datasets based on the palmer drought severity index. J. Hydrometeorol.11(4): 1033–1043.

Wen, K.G., Shi, Y.G. 2006.Chinese Meteorological Disaster Dictionary: Xinjiang Volume. Beijing: Meteorological Press.

Wang, Y.F., Shen, Y.J., Sun, F.B., Chen, Y.N., 2014. Evaluating the vegetation growing season changes in the arid region of northwestern China. Theor. Appl. Climatol. 118 (3), 569–579.

Wang, B., Xu, G., Li, P., Li, Z., Zhang, Y., Cheng, Y., 2020. Vegetation dynamics and their relationships with climatic factors in the Qinling Mountains of China. Ecol. Ind. 108 https://doi.org/10.1016/j.ecolind.2019.105719.

Willmott, C.J., Rowe, C.M., Mintz, Y., 1985. Climatology of the terrestrial seasonal water cycle. J. Climatol. 5 (6), 589–606.

Yang, Y., Chen, Y., Li, W., Yu, S., Wang, M., 2012. Climatic change of inland river basin in an arid area: A case study in northern Xinjiang, China. Theor. Appl. Climatol. 107 (1), 143–154.

Yao, J.Q., Chen, Y.N., Zhao, Y., Mao, W.Y., Xu, X.B., Liu, Y., et al., 2018. Response of vegetation NDVI to climatic extremes in the arid region of Central Asia: A case study in Xinjiang, China. Theor. Appl. Climatol. 131 (3), 1503–1515.

Zhou, D., Zhang, B., Luo, J., Zhang, C., Wang, D., 2014. SPEI based intensity characteristics and cause analysis of drought in north China during recent 50 years. J. Nat. Disasters 23 (4), 192–202.

Zargar, A., Sadiq, R., Naser, B., Khan, F.I., 2011. A review of drought indices. Environ. Rev. 19, 333–349.

Zhang, L.Y., Wang, Y., Chen, Y.N., 2020. Spatial and temporal distribution characteristics of drought in Central Asia based on SPEI index. Arid Zone Res. 37 (02), 331–339.

Zhang, Q., Li, J., Singh, V.P., Bai, Y., 2012. SPI-based evaluation of drought events in Xinjiang, China. Natural Hazards. 64 (1), 481–492.

Zhang, Q., Sun, P., Li, J., Xiao, M., Singh, V.P., 2015. Assessment of drought vulnerability of the tarim river basin, xinjiang, china. Theor. Appl. Climatol. 121 (1–2), 337–347.

Zhang, B.Q., Wu, P., Zhao, X.N., Wang, Y.B., Gao, X.D., Cao,, X.C., 2013. A drought hazard assessment index based on the VIC–PDSI model and its application on the Loess Plateau, China. Theor. Appl. Climatol. 114 (1), 125–138.

Zhang, Y., Chu, X.Z., Yang, S.M., Guo, C., 2019. Climate Change in North Xinjiang in recent 56 years. Arid Zone Res. 36 (01), 215–222.

Zhao, B., Zhang, B., Shi, C., Liu, J., Jiang, L., 2019. Comparison of the global energy cycle between chinese reanalysis interim and ECMWF reanalysis. J. Meteorol. Res. 33 (3), 563–575.